

# Stability of Steel Columns Subjected to Earthquake and Fire Loads

Mehrdad Memari, A.M.ASCE<sup>1</sup>; Hussam Mahmoud, M.ASCE<sup>2</sup>; and Bruce Ellingwood, Dist.M.ASCE<sup>3</sup>

**Abstract:** Assessing the stability of steel building frames exposed to fire conditions is challenging because of the need to consider the elevated temperature properties of steel, nonuniform heating of structural members, and large deformational demands on the frames. This challenge is further intensified if the stability of the frame is also influenced by the lateral forces of an earthquake that preceded the fire. Although there has been significant progress recently in simulating the response of frames using finite-element methods, there is a need for computationally efficient tools that would minimize the modeling effort and allow for accurate and rapid assessment so that a large number of simulations can be conducted. To this end, the present study aims to develop a framework for conducting a stability analysis of steel columns subjected to demands imposed by lateral loading followed by fire. A nonlinear formulation is proposed to assess the stability of W-shaped steel columns under multihazard loading scenarios. Results from the proposed formulation show good agreement with available strength design equations of steel columns at ambient and elevated temperatures. This computationally efficient tool can be used to investigate the effects of a wide variety of variables on the stability of steel columns subjected to fire and fire following earthquakes. DOI: 10.1061/(ASCE)ST.1943-541X.0001909. © 2017 American Society of Civil Engineers.

**Author keywords:** Steel columns; Fire following earthquake; Nonuniform temperature distribution; Stability analysis;  $P$ - $\Delta$  effects; Temperature-dependent material properties; Analysis and computation.

## Introduction

Significant progress has been made recently in the development of analytical, numerical, and experimental tools that can be used to evaluate the response of steel structural members and frames under fire loads. Despite this progress, many challenges in evaluating structural response under fire loading remain owing to the significant geometrical nonlinearity and temperature-dependent material inelasticity that must be considered in the structural analysis. This is particularly the case when assessing the behavior of axially loaded members due to the presence of low or negative stiffness at the onset of instability. The stability of axially loaded members, particularly columns, under elevated temperatures has been the focus of several studies (Franssen et al. 1998; Takagi and Deierlein 2007; Agarwal and Varma 2011) because columns are key components in resisting gravity loads in a building system.

A review of the literature indicates that many experimental and numerical studies have been conducted to investigate the stability of isolated steel columns exposed to fire loads (e.g., Vandamme and Janss 1981; Franssen et al. 1998; Ali and O'Connor 2001; Takagi and Deierlein 2007; Tan and Yuan 2009; Agarwal and Varma 2011; Agarwal et al. 2014). Memari and Mahmoud (2014) and

Memari et al. (2014) conducted nonlinear finite-element analyses to evaluate the performance of steel moment-resisting frames under fire and fire following earthquakes, respectively. These studies highlighted the need to enhance understanding of the response of steel columns subjected to nonuniform temperature over their length and interstory drift. The brief discussion that follows of the two most recent and relevant studies on steel column buckling under fire (Takagi and Deierlein 2007; Agarwal and Varma 2011) will set the stage for introducing a new analytical model for evaluating the response of W-shaped steel columns under the effects of lateral demand followed by fire loading.

Takagi and Deierlein (2007) evaluated the *AISC 2005 Specification* [AISC 360-05 (AISC 2005)] and *Eurocode 3* (CEN 2005) provisions for the design of isolated W-shaped steel columns under elevated temperatures that were uniform along the column length. Numerical models of columns were developed that accounted for residual stresses, local and overall buckling, and material inelasticity. Temperature-dependent material properties were adopted from *Eurocode 3* (CEN 2005). Initial geometric imperfections were also considered in the numerical models. It was concluded that using the column design equations in Chapter E when designing axially loaded members under elevated temperatures, modifying only the material properties for elevated temperatures, was highly nonconservative. The outcome of this study was equation (A-4-2) in Appendix 4 of the *AISC 2010 Specification* [AISC 360-10 (AISC 2010)]—also available in *AISC 2016 Specification* [AISC 360-16 (AISC 2016)]—for W-shaped steel columns exposed to uniform temperatures over their lengths.

Subsequently, Agarwal and Varma (2011) conducted finite-element analyses to evaluate the effects of slenderness and rotational restraints on the buckling of W-shaped steel columns at uniform elevated temperatures. Shell elements were used to create numerical models of columns because of their ability to capture local buckling and inelastic flexural-torsional buckling and to accommodate the specified residual stress distribution. Initial geometric imperfections, representing out-of-straightness, were included

<sup>1</sup>Postdoctoral Fellow, Dept. of Civil and Environmental Engineering, Colorado State Univ., Fort Collins, CO 80523-1372. E-mail: Mehrdad.Memari@Colostate.Edu

<sup>2</sup>Associate Professor, Dept. of Civil and Environmental Engineering, Colorado State Univ., Fort Collins, CO 80523-1372 (corresponding author). E-mail: Hussam.Mahmoud@Colostate.Edu

<sup>3</sup>Professor, Dept. of Civil and Environmental Engineering, Colorado State Univ., Fort Collins, CO 80523-1372. E-mail: Bruce.Ellingwood@Colostate.Edu

Note. This manuscript was submitted on February 7, 2017; approved on June 7, 2017; published online on October 23, 2017. Discussion period open until March 23, 2018; separate discussions must be submitted for individual papers. This paper is part of the *Journal of Structural Engineering*, © ASCE, ISSN 0733-9445.

in the models, as were local imperfections. As with the earlier Takagi and Deierlein (2007) study, temperature-dependent stress-strain curves from *Eurocode 3* (CEN 2005) were employed in the numerical models. This study resulted in new design equations for simply supported columns with uniform temperature distributions over their lengths, considering an equivalent bilinear material behavior. The effects of rotational restraints, provided by continuity with cooler columns above and below the column of interest in a structural frame, were also included in the proposed design equations. The outcome of this study is available in the Commentary of Appendix 4 of the *AISC 2016 Specification* [AISC 360-16 (AISC 2016)].

The studies by Takagi and Deierlein (2007) and Agarwal and Varma (2011) showed that the computational efforts associated with analyzing the stability of columns at elevated temperatures were significant, and both studies introduced a set of assumptions and simplifications to reduce the number of analyses to minimize the computational efforts. For instance, they did not include the effects of nonuniform longitudinal temperature profiles, various boundary conditions, and  $P$ - $\Delta$  effects. There remains a need for relatively simple tools that can be utilized to evaluate the instability of columns under multiple demands and can account for the various inelastic and geometrically nonlinear features associated with column behavior under elevated temperatures.

Such tools are developed in this study, in which an analytically nonlinear formulation is developed to perform a stability analysis of  $W$ -shaped steel columns subjected to initial imperfections,  $P$ - $\Delta$  effects, and nonuniform distributions of temperature along the column lengths. This formulation takes into account the residual stress distribution in  $W$ -shaped hot-rolled steel sections, initial out-of-straightness and out-of-plumbness in steel columns, temperature-dependent material properties, residual interstory drift caused by lateral demands, and specified boundary conditions, i.e., pinned-pinned, fixed-fixed, and fixed-pinned. The results of the proposed approach are verified by comparisons with previous studies.

The results highlight the importance of details of the material modeling and  $P$ - $\Delta$  effects on the instability of steel columns exposed to either uniform or nonuniform longitudinal elevated temperature profiles. The identification of fire scenarios is outside the scope of this study because the occupancy of the steel building frame is not specified. However, the column temperatures considered in the case studies are typical of the temperatures that develop in steel columns designed in accordance with Appendix 4 of the *AISC 2016 Specification* [AISC 360-16 (AISC 2016)].

## Second-Order Finite-Element Formulation

### Fundamental Equations

The proposed analysis of a geometrically nonlinear response of a beam-column element subjected to a nonuniform temperature distribution along its length is based on Euler-Bernoulli beam theory and is an extension of results obtained by Carol and Murcia (1989) and Memari and Attarnejad (2010). A finite element of length  $L$ , shown in Fig. 1(a), is assumed to have a nonuniform temperature distribution, with  $T_i$  and  $T_j$  being the nodal temperatures at either end, while the temperature across the section is uniform. The assumption of a uniform temperature in the cross section is based on a previous study by NIST in which it was shown that the variation in the cross-sectional temperature was minimal (Phan et al. 2010). This assumption is reasonable for unprotected steel members, as well as for steel members with uniform protection from all sides when they are uniformly subjected to fire load from all sides. An example of such a case would be an interior column in a building that is subjected to fire from all sides owing to a multiple-compartment fire on a given floor.

Since the elastic modulus of steel is a function of temperature and degrades at elevated temperatures, the nodal temperature at each end of the element will result in temperature-dependent

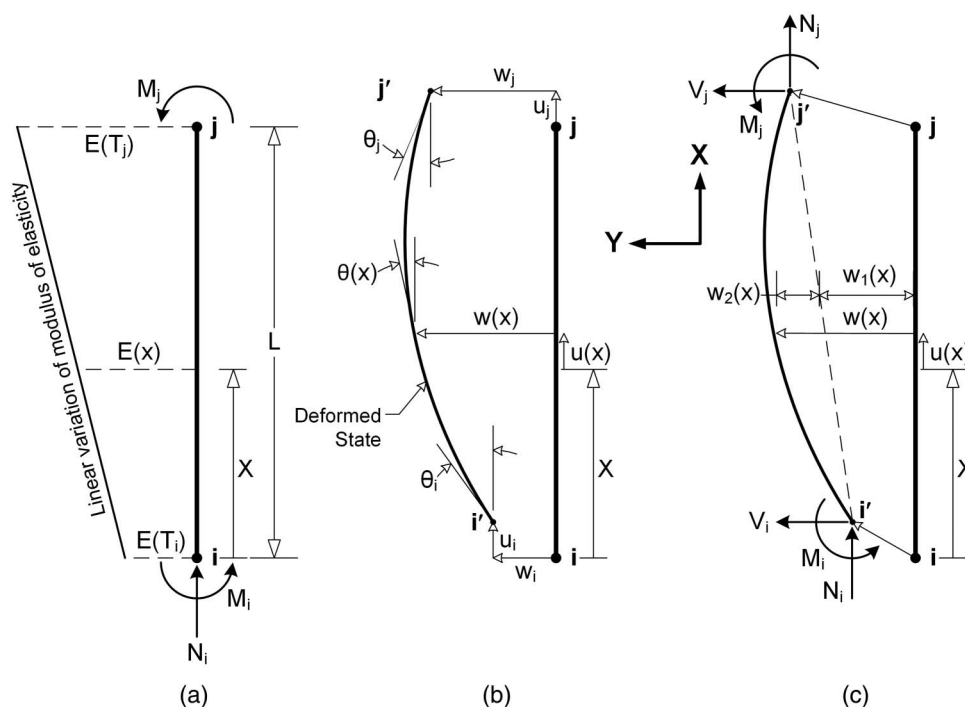


**Fig. 1.** (a) Finite element subjected to nonuniform longitudinal temperature along with applied external axial force,  $N_i$ , and bending moments,  $M_i$  and  $M_j$ ; (b) deformed state of element with all nodal deformation variables; (c) deformed state of element with all nodal force variables

moduli of elasticity  $E(T_i)$  and  $E(T_j)$ , as shown in Fig. 1(a). In this study, a linear variation of a temperature-dependent modulus of elasticity is assumed along the length of the finite element. The entire column can be divided into elements that are sufficiently short that the linear variation along each element allows the non-linear variation along the entire length of the column to be captured. The modulus of elasticity along the length of the finite element at coordinate  $x$ ,  $E(x)$ , can therefore be written

$$E(x) = E(T_i) \left( 1 + \frac{\zeta x}{L} \right) \quad (1a)$$

where  $L$  = length of finite element, and  $\zeta$  is calculated as follows:

$$\zeta = \frac{E(T_j)}{E(T_i)} - 1 \quad (1b)$$

If the temperature is constant along the length of the element,  $\zeta = 0$ .

Fig. 1(a) shows that three external nodal actions—axial force at node  $i$  and bending moments at nodes  $i$  and  $j$ —are applied to the beam-column element. Figs. 1(b and c) show the deformed state of this element with full nodal deformations and applied external nodal actions, respectively. In accordance with the deformed state of the element, Fig. 1(b), the kinematic (strain-displacement) equations can be written in the following matrix form:

$$\begin{bmatrix} -(u_j - u_i) \\ \frac{w_j - w_i}{L} - \theta_i \\ \theta_j - \frac{w_j - w_i}{L} \end{bmatrix} = \int_0^L \begin{bmatrix} 1 & 0 \\ 0 & 1 - \frac{x}{L} \\ 0 & \frac{x}{L} \end{bmatrix} \begin{bmatrix} \varepsilon \\ \varphi \end{bmatrix} dx \quad (2a)$$

$$\mathbf{u} = \int_0^L \mathbf{\Omega}^T \cdot \boldsymbol{\gamma} dx \quad (2b)$$

where  $\varepsilon$  and  $\varphi$  = axial strain at neutral axis of element cross section and element curvature, respectively. Other variables in Eq. (2a) are shown in Fig. 1(b). The matrix form of the kinematic equations is written in a more compact form in Eq. (2b), where  $\mathbf{u}$  is a vector of relative displacements and rotations,  $\boldsymbol{\gamma}$  is a vector of strains, and  $\mathbf{\Omega}$  is a matrix that transforms strains into displacements and rotations.

Cross-sectional forces can be obtained based on applied external nodal forces and moments using equilibrium equations per Eq. (3a) in what follows. To include the second-order moments due to the deflection of column centerline with respect to its chord, often referred to as the  $P$ - $\delta$  effect, a vector of forces due to the deformed state of the beam-column element, shown in Fig. 1(c), is added to the nodal equilibrium equations:

$$\begin{bmatrix} N(x) \\ M(x) \end{bmatrix} = \begin{bmatrix} 1 & 0 & 0 \\ 0 & 1 - \frac{x}{L} & \frac{x}{L} \end{bmatrix} \begin{bmatrix} N_i \\ M_i \\ M_j \end{bmatrix} + \begin{bmatrix} 0 \\ -N_i \cdot w_2(x) \end{bmatrix} \quad (3a)$$

$$\mathbf{R}(\mathbf{x}) = \mathbf{\Omega} \cdot \mathbf{f} + \mathbf{R}_2(\mathbf{x}) \quad (3b)$$

where  $w_2(x)$  = out-of-straightness curvature of the beam-column that causes the  $P$ - $\delta$  effects. The compact format of the matrix equation, Eq. (3b), indicates that  $\mathbf{R}_2(\mathbf{x})$  is a vector of cross-sectional forces developed because of the inclusion of the  $P$ - $\delta$  effect. The vector  $\mathbf{f}$  represents the applied external nodal actions, and  $\mathbf{\Omega}$  is a matrix that correlates the applied external nodal actions to those

developed internally in the cross section. Note that the matrix  $\mathbf{\Omega}$  appears in both the kinematic and equilibrium equations.

The cross-sectional strain and curvature are related to the cross-sectional forces using constitutive law per the following Eqs. (4a) and (4b), under the assumption that the element responds elastically to nodal forces:

$$\begin{bmatrix} N(x) \\ M(x) \end{bmatrix} = \begin{bmatrix} E(x)A & 0 \\ 0 & E(x)I \end{bmatrix} \begin{bmatrix} \varepsilon \\ \varphi \end{bmatrix} \quad (4a)$$

$$\mathbf{R}(\mathbf{x}) = \mathbf{k}_s(\mathbf{x}) \cdot \boldsymbol{\gamma} \quad (4b)$$

in which  $\mathbf{k}_s(\mathbf{x})$  = section stiffness matrix. The variation in the elastic modulus along the column length caused by the nonuniform temperature distribution is reflected in Eq. (4). This is one of the most important features of the present formulation since a constant modulus of elasticity would imply no variation in temperature along the length. Substituting the longitudinal linear variation of the elastic modulus, Eq. (1), into the equation representing  $\mathbf{k}_s(\mathbf{x})$  leads to Eq. (5):

$$\mathbf{k}_s(\mathbf{x}) = E(T_i) \left( 1 + \frac{\zeta x}{L} \right) \begin{bmatrix} A & 0 \\ 0 & I \end{bmatrix} \quad (5)$$

which clearly indicates that the section stiffness varies along the length of element as a function of temperature (elastic modulus).

### First- and Second-Order Stiffness Matrices

The first-order and geometric stiffness matrices necessary for the stability analysis can be extracted from the kinematic, equilibrium, and constitutive law equations. First, substituting the equilibrium, Eq. (3b), and constitutive, Eq. (4b), equations into the kinematic equation, Eq. (2b), results in

$$\mathbf{u} = \int_0^L \mathbf{\Omega}^T \mathbf{k}_s^{-1} \mathbf{\Omega} \mathbf{f} dx + \int_0^L \mathbf{\Omega}^T \mathbf{k}_s^{-1} \mathbf{R}_2(\mathbf{x}) dx \quad (6)$$

Eq. (6) can be rearranged based on  $\mathbf{f}$ , leading to

$$\mathbf{f} = \boldsymbol{\eta} \cdot \mathbf{u} + \mathbf{f}_2 \quad (7)$$

in which

$$\boldsymbol{\eta} = \left( \int_0^L \mathbf{\Omega}^T \mathbf{k}_s^{-1} \mathbf{\Omega} dx \right)^{-1} \quad (8a)$$

$$\mathbf{f}_2 = -\boldsymbol{\eta} \int_0^L \mathbf{\Omega}^T \mathbf{k}_s^{-1} \mathbf{R}_2(\mathbf{x}) dx \quad (8b)$$

where stiffness  $\boldsymbol{\eta}$  relates the vector of relative displacements and rotations,  $\mathbf{u}$ , to the vector of applied external actions,  $\mathbf{f}$ , and  $\mathbf{f}_2$  represents nodal actions resulting from second-order  $P$ - $\delta$  effects. If the  $\mathbf{\Omega}$  and  $\mathbf{k}_s^{-1}$  matrices are substituted into Eq. (8a),  $\boldsymbol{\eta}$  will become

$$\boldsymbol{\eta} = \left( \int_0^L \frac{1}{E(T_i)(1 + \frac{\zeta x}{L})} \begin{bmatrix} \frac{1}{A} & 0 & 0 \\ 0 & \frac{(1 - \frac{x}{L})^2}{I} & \frac{(1 - \frac{x}{L})\frac{x}{L}}{I} \\ 0 & \frac{(1 - \frac{x}{L})\frac{x}{L}}{I} & \frac{(\frac{x}{L})^2}{I} \end{bmatrix} dx \right)^{-1} \quad (9)$$

As a final step, the vector of applied nodal forces and moments,  $\mathbf{f}$ , and the vector of relative displacements and rotations,  $\mathbf{u}$ , must be

related to the full vector of nodal actions and deformations,  $\mathbf{F}$  and  $\mathbf{U}$ , respectively:

$$\mathbf{F} = [N_i \quad V_i \quad M_i \quad N_j \quad V_j \quad M_j]^T \quad (10a)$$

$$\mathbf{U} = [u_i \quad w_i \quad \theta_i \quad u_j \quad w_j \quad \theta_j]^T \quad (10b)$$

A transformation matrix,  $\mathbf{\Gamma}$ , defined by

$$\mathbf{\Gamma} = \begin{bmatrix} 1 & 0 & 0 \\ 0 & -\frac{1}{L} & \frac{1}{L} \\ 0 & -1 & 0 \\ -1 & 0 & 0 \\ 0 & \frac{1}{L} & -\frac{1}{L} \\ 0 & 0 & 1 \end{bmatrix} \quad (11)$$

can be used to relate  $\mathbf{f}$  and  $\mathbf{u}$  to  $\mathbf{F}$  and  $\mathbf{U}$ , respectively, per Eq. (12). Note that the moments caused by the  $P$ - $\delta$  effects have been considered in Eq. (7) via vector  $\mathbf{f}_2$ . Therefore, Eq. (12a) includes the effects of moments; however, the shear forces caused by the  $P$ - $\delta$  effects are missing. Therefore, a new vector of nodal shear forces,  $\mathbf{F}_2$ , is added to  $\mathbf{F}$ , as shown in Eq. (12a). This new vector, shown in Eq. (13), considers the shear forces to be proportional to the axial force caused by  $P$ - $\delta$  effects:

$$\mathbf{F} = \mathbf{\Gamma} \cdot \mathbf{f} + \mathbf{F}_2 \quad (12a)$$

$$\mathbf{u} = \mathbf{\Gamma}^T \cdot \mathbf{U} \quad (12b)$$

$$\mathbf{F}_2 = \begin{bmatrix} 0 & N_i \frac{w_j - w_i}{L} & 0 & 0 & -N_i \frac{w_j - w_i}{L} & 0 \end{bmatrix}^T \quad (13)$$

Substituting Eqs. (7) and (12b) into Eq. (12a) yields

$$\mathbf{F} = \mathbf{\Gamma} \cdot (\boldsymbol{\eta} \mathbf{u} + \mathbf{f}_2) + \mathbf{F}_2 = \mathbf{\Gamma} \boldsymbol{\eta} \mathbf{\Gamma}^T \mathbf{U} + \mathbf{\Gamma} \mathbf{f}_2 + \mathbf{F}_2 \quad (14)$$

As can be seen from Eq. (14), the full vector of nodal actions,  $\mathbf{F}$ , has been related to the full vector of nodal deformations via the first term; therefore, the stiffness matrix of an element,  $\mathbf{K}$ , with nonuniform longitudinal temperature can be defined by

$$\mathbf{K} = \mathbf{\Gamma} \boldsymbol{\eta} \mathbf{\Gamma}^T \quad (15)$$

The term  $\boldsymbol{\eta}$  in the element stiffness matrix reflects the effects of temperature variation along the length of the beam-column element. The second and third terms in Eq. (14) represent the geometric stiffness matrix of the element,  $\mathbf{K}_G$ :

$$\mathbf{K}_G \mathbf{U} = \mathbf{\Gamma} \mathbf{f}_2 + \mathbf{F}_2 \quad (16)$$

The overall second-order elastic stiffness can be written in classic form  $\mathbf{K} = \mathbf{K} + \mathbf{K}_G$ .

All vectors and matrices in Eq. (16) were established with the exception of  $\mathbf{R}_2(\mathbf{x})$ , which is embedded in Eq. (8) defining  $\mathbf{f}_2$ . However, only  $w_2(x)$  is needed to define  $\mathbf{R}_2(\mathbf{x})$ , which can be obtained using the compatibility equation of the element in its deformed state according to Fig. 1(b). Defining  $w(x)$  in terms of nodal displacements and rotations results in the determination of  $w_2(x)$  through the following steps:

$$w(x) = w_i + \theta_i x + \int_0^x \varphi(x - \tau) d\tau \quad (17a)$$

$$w_1(x) = w_i + \frac{w_j - w_i}{L} x \quad (17b)$$

$$\begin{aligned} w_2(x) &= w(x) - w_1(x) \\ &= \theta_i x + \frac{w_i - w_j}{L} x + \int_0^x [0 \quad x - \tau] \begin{bmatrix} \varepsilon \\ \varphi \end{bmatrix} d\tau \end{aligned} \quad (17c)$$

$$w_2(x) = \theta_i x + \frac{w_i - w_j}{L} x + \int_0^x \boldsymbol{\beta} \boldsymbol{\gamma} d\tau \quad (17d)$$

$$w_2(x) = \theta_i x + \frac{w_i - w_j}{L} x + \int_0^x \boldsymbol{\beta} \mathbf{k}_s^{-1} \boldsymbol{\Omega} \boldsymbol{\eta} \mathbf{\Gamma}^T \mathbf{U} d\tau \quad (17e)$$

The inclusion of matrix  $\boldsymbol{\eta}$  in Eq. (17e) inherently accounts for the effects of temperature variation along the element length on the geometric stiffness matrix of the element.

## Analysis of Column Stability under Elevated Temperatures

### Finite-Element Analysis

This section presents details of the finite-element analysis used to obtain the critical buckling stress at instability for a column subjected to either a uniform or nonuniform temperature distribution over its length. Fig. 2 shows a schematic description of the finite-element model of a steel column with a nonuniform distribution of temperature over its length. All columns analyzed in this study are divided into 50 identical elements in length, regardless of the uniformity of the temperature distribution. Although a mesh study indicated that 25–30 elements were sufficient to achieve the required level of accuracy, it was decided to use 50 elements since the increase in computational demand, compared to what is required for 25 elements, is negligible. The assemblage of stiffness matrices (elastic and geometric) of all 50 elements results in the stiffness matrix of a column, as described in what follows.

As shown in Fig. 2(a), initial out-of-straightness is considered in the geometry of the columns analyzed. The out-of-straightness is modeled by introducing a single sinusoidal curve along the column length such that a maximum displacement of  $0.001L_c$ —as per Comm. C2, in the *AISC 2016 Specification* [AISC 360-16 (AISC 2016)]—is located at midheight of the column, where  $L_c$  is the length of the column. As shown in Fig. 2(c), the rotation angle of each element ( $\alpha$ ) in global coordinates resulting from the initial out-of-straightness is considered separately in generating the elastic and geometric stiffness matrices of the element. The transformation matrix of Eq. (18) is used to obtain the stiffness matrices in accordance with the global coordinates considering the element angle ( $\alpha$ ) as shown in Eqs. (19a) and (19b):

$$\mathbf{T} = \begin{bmatrix} \cos \alpha & \sin \alpha & 0 & 0 & 0 & 0 \\ -\sin \alpha & \cos \alpha & 0 & 0 & 0 & 0 \\ 0 & 0 & 1 & 0 & 0 & 0 \\ 0 & 0 & 0 & \cos \alpha & \sin \alpha & 0 \\ 0 & 0 & 0 & -\sin \alpha & \cos \alpha & 0 \\ 0 & 0 & 0 & 0 & 0 & 1 \end{bmatrix} \quad (18)$$

$$\mathbf{K}_\alpha = \mathbf{T}^T \mathbf{K} \mathbf{T} \quad (19a)$$



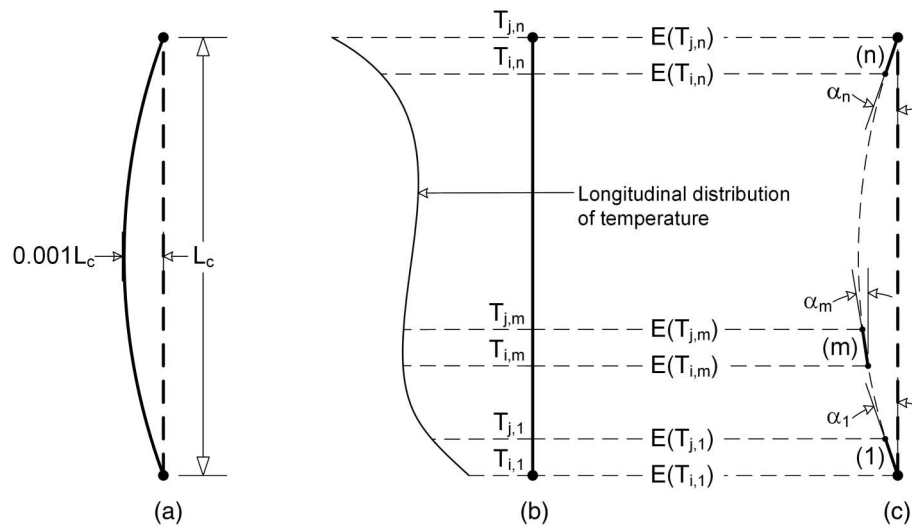


**Fig. 2.** (a) Inclusion of out-of-straightness initial imperfection with single sinusoidal curve along length of column; (b) nonuniform distribution of temperature along column length; (c) schematic explanation of finite-element analysis considering angle of elements

$$\mathbf{K}_{G,\alpha} = \mathbf{T}^T \mathbf{K}_G \mathbf{T} \quad (19b)$$

where  $\mathbf{K}_\alpha$  and  $\mathbf{K}_{G,\alpha}$  = first-order and geometric stiffness matrices in the global coordinate system. The effect of initial out-of-plumbness ( $P-\Delta$ ) imperfection is also included explicitly in the finite-element analysis. This is realized through introducing an initial out-of-plumbness of  $0.001L_c$ —below the allowable limit of  $0.002L_c$  as per Comm. C2 in the *AISC 2016 Specification* [AISC 360-16 (AISC 2016)]—at the top end of the column and calculating the lateral sway for the remaining nodes, assuming a straight column. Following this step, the lateral nodal displacements are multiplied by the applied axial force to calculate the corresponding nodal moments, which are then assembled with the applied axial force to form the entire action vector on the column.

The nodal temperatures at the ends of each element are also considered in generating the stiffness matrices described in Figs. 2(b and c). The modulus of elasticity, corresponding to the nodal temperatures, can be obtained from available codes, for instance *Eurocode 3* (CEN 2005) or the *AISC 2016 Specification* [AISC 360-16 (AISC 2016)]. To determine the critical buckling stress causing column instability, the applied compressive force is increased incrementally until the onset of buckling in the column. A maximum loading increment ( $\Delta P$ ) of 2.45 kN (1 kip) is adopted in this study. A compact W14X90 section, fabricated from ASTM A992 structural steel [ASTM A992/A992M (ASTM 2015)], is selected for the finite-element analyses.

### Inelastic Buckling

As indicated in the *AISC 2016 Specification* [AISC 360-16 (AISC 2016)], slender columns with a slenderness ratio ( $\lambda = L/r$ ) less than  $4.71\sqrt{\frac{E}{F_y}}$  at ambient temperature are susceptible to inelastic buckling, while columns with a slenderness ratio greater than  $4.71\sqrt{\frac{E}{F_y}}$  buckle elastically. Therefore, it is important that this distinction be captured in the finite-element analysis of the column. This is realized by defining two independent limit states. For inelastic buckling, six reference points (RPs) are specified over the cross section of the column, as shown in Fig. 3(a), and the stresses developed at these six RPs are calculated in all elements at each loading increment using Eq. (20):

$$\sigma(n, m) = \max\left(\frac{P(m)}{A} + \frac{M(n, m) \cdot y_{1:6}}{I}\right) \quad (20)$$

where  $\sigma(n, m)$  and  $M(n, m)$  = maximum developed compressive stress and the bending moment, respectively, at node  $n$  in increment  $m$ ;  $P(m)$  = applied axial compressive force at increment  $m$ ;  $y_{1:6}$  = distance from the six RPs to the neutral axis of the cross section, as shown in Fig. 3(a); and  $A$  and  $I$  are the cross-sectional area and moment of inertia, respectively.

The onset of compressive yielding at any of these six RPs, based on the yield stress for the temperature at that section, is chosen as the limit state for inelastic buckling in accordance with Eq. (21):

$$\chi(m) = \frac{\sigma(n, m)}{F_y(n)} \quad (21)$$

where  $\chi(m)$  = maximum ratio of developed compressive stress,  $\sigma(n, m)$ , to yield stress at node  $n$ ,  $F_y(n)$ , at loading increment  $m$ .

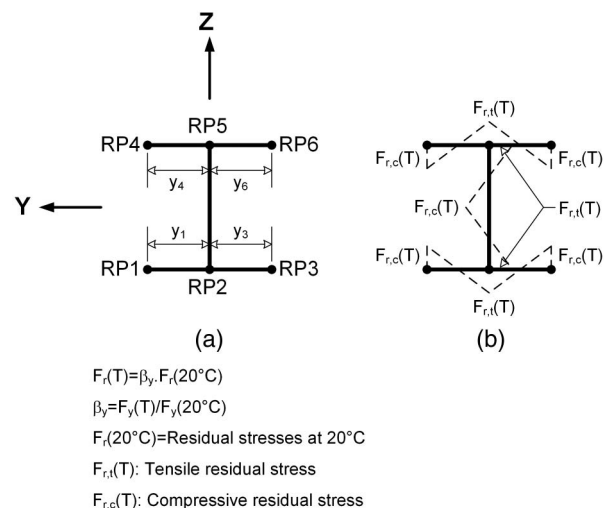


**Fig. 3.** (a) Six reference points (RPs) in W-shaped steel section; (b) distribution of residual stresses in W-shaped hot-rolled steel sections

It should be noted that  $F_y(n)$  is not constant and depends on the nodal temperature. Furthermore, the calculated stress in the cross section is influenced not only by the applied load but also by any residual stresses that might be present, modeled by the residual stress field shown in Fig. 3(b). It is assumed that the maximum thermally induced residual stresses are 70 MPa (approximately  $0.2F_y$ ) at ambient temperature according to assumption made by Takagi and Deierlein (2007). The reduction factor for yield stress at elevated temperatures is also used to reduce the intensity of the residual stresses in the cross section. This assumption was also made by Takagi and Deierlein (2007) and allows the authors to compare the results of the present study with the aforementioned article. Lastly, the inelastic critical buckling stress,  $F_{cr}$ , is determined using Eq. (22), when the value of  $\chi(m)$ , in one of the sections, reaches a limit of 0.99:

$$F_{cr} = \frac{P(m)}{A} \quad (22)$$

### Elastic Buckling

The lateral stiffness of the steel column under the applied compressive load defines the limit state for elastic buckling. In this limit state, the applied compressive load and maximum deflection of the column are recorded at each increment. The lateral stiffness of the column in increment  $m$ ,  $\kappa(m)$ , is obtained using Eq. (23):

$$\kappa(m) = \frac{P(m) - P(m-1)}{d(m) - d(m-1)} \quad (23)$$

where  $P(m)$ ,  $P(m-1)$ ,  $d(m)$ , and  $d(m-1)$  = applied compressive forces and maximum deflections, respectively, of the column in increments  $m$  and  $m-1$ . Once the lateral stiffness of the column at a given loading increment is computed, it is then compared to the initial lateral stiffness of the column,  $\kappa(1)$ , which is calculated based on the first increment of loading. This is performed using

$$\rho(m) = \frac{\kappa(m)}{\kappa(1)} \quad (24)$$

where  $\rho(m)$  = reduction in column lateral stiffness in  $m$ th increment in comparison to the initial lateral stiffness,  $\kappa(1)$ . Theoretically, Euler elastic buckling for a concentrically loaded column takes place when  $\rho(m)$  reaches zero. However, an initial assessment of the method herein indicates that the onset of elastic buckling is reached when the column loses 96% or more of its initial lateral stiffness. Therefore, the elastic buckling is determined when  $\rho(m)$  is at 4% or less in the  $m$ th increment of loading. Eq. (22) is also used here to calculate the elastic critical buckling stress,  $F_{cr}$ .

### Temperature-Dependent Material Modeling

In this study, the stress-strain curve for ASTM A992 structural steel [ASTM A992/A992M (ASTM 2015)] is assumed to be elastic-perfectly plastic at ambient temperature. However, at elevated temperatures, the transition from elastic to inelastic material behavior utilized in the stability analysis has shown a significant effect on the calculated critical buckling stress of steel columns at elevated temperatures (Takagi and Deierlein 2007; Agarwal and Varma 2011). Three essential mechanical properties of structural steel are considered in the instability analysis of columns exposed to elevated temperatures: modulus of elasticity ( $E$ ), proportional limit ( $F_p$ ), and yield stress ( $F_y$ ). Variations of  $E$ ,  $F_p$ , and  $F_y$  as a function of temperature according to Eurocode 3 (CEN 2005),

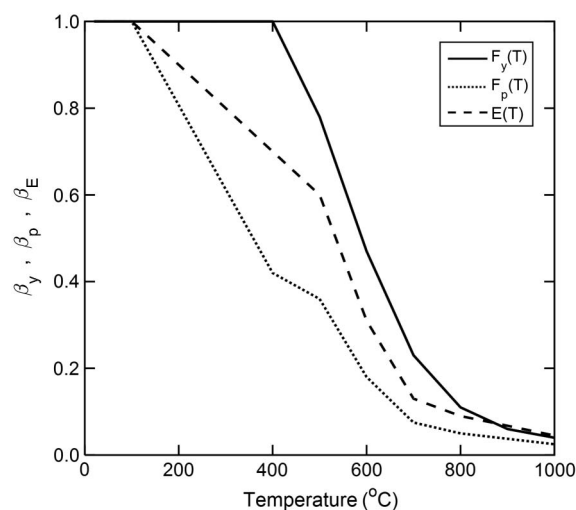


**Fig. 4.** Variations of  $E$ ,  $F_p$ , and  $F_y$  as a function of temperature per Eurocode 3 (CEN 2005), normalized to their values at ambient temperature, are denoted by  $\beta_E$ ,  $\beta_p$ , and  $\beta_y$ , respectively

normalized to their values at ambient temperature, are denoted by  $\beta_E$ ,  $\beta_p$ , and  $\beta_y$ , respectively, and are shown in Fig. 4. The analysis herein does not consider fire protection of the structural steel material. It is therefore conservative in assuming that the temperature is applied to the full column as opposed to a specific region where the fire protection has been damaged or removed.

Four alternative material modeling approaches are considered for ASTM A992 structural steel [ASTM A992/A992M (ASTM 2015)] as shown in Fig. 5. First, the temperature-dependent mechanical properties of steel material are modeled exactly as in Eurocode 3 (CEN 2005), as shown in Fig. 5(a). This material modeling inherently considers thermal creep effects, as indicated by the curvilinear behavior of material at elevated temperatures. As noted previously, this material modeling approach was implemented by Takagi and Deierlein (2007). Second, an actual curvilinear stress-strain curve of steel material at elevated temperatures is idealized with the bilinear relation shown in Fig. 5(b). In this approach, the equivalent modulus of elasticity,  $E_{eq}(T)$ , and yield stress,  $F_{y,eq}(T)$ , are computed such that the two hatched areas in Fig. 5(b) are equal. This approach has been used by Agarwal and Varma (2011). Third, a temperature-dependent elastic-perfectly plastic stress-strain curve is considered with no consideration of the effects of proportional limit ( $F_p$ ), as shown in Fig. 5(c). Fourth, a trilinear stress-strain curve is implemented, as shown in Fig. 5(d). In this approach, the temperature-dependent modulus of elasticity is adopted from Eurocode 3 (CEN 2005) with no changes; however, a new effective yield stress,  $F_{ye}(T)$ , is defined such that two hatched areas in Fig. 5(d) are identical. These four approaches are referred to in the next sections of this article as Material Models (a)–(d). The variations in  $E$ ,  $F_p$ , and  $F_y$  as a function of temperature, described by  $\beta_E$ ,  $\beta_p$ , and  $\beta_y$  for the four different reference stress-strain curves are summarized in Table 1.

### Validation of Proposed Analysis

A set of analyses is conducted to illustrate the column stability analysis approach presented herein and to compare the buckling stresses predicted with this approach to those predicted by other investigators under similar temperature and constitutive material conditions. This includes examination of buckling stress of a

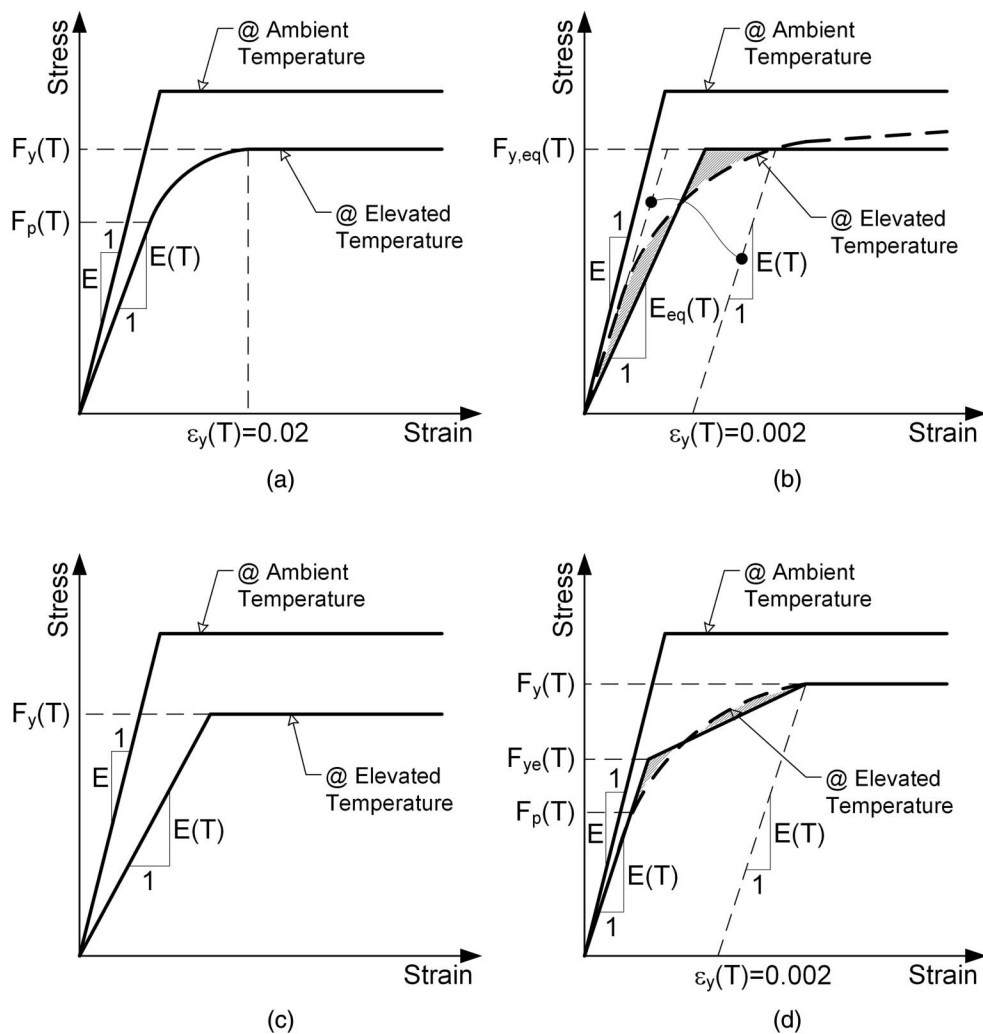


**Fig. 5.** Material modeling: (a) *Eurocode 3* (CEN 2005) employed by Takagi and Deierlein (2007); (b) Agarwal and Varma (2011); (c) elastic–perfectly plastic; (d) trilinear equivalent model

pinned–pinned column at ambient and elevated temperatures using the W14X90 steel column. While the developed formulation can account for any restraints at the column ends, only pinned–pinned boundary conditions are used so that a direct comparison can be used against existing code provisions, which were developed using pinned–pinned boundary conditions. Details of the column evaluated are shown in Fig. 6.

**Table 1.** Summary of Variations in  $\beta_E$ ,  $\beta_y$ , and  $\beta_p$  for the Four Different Stress-Strain Curves Considered

Temperature (°C)	Material (a)			Material (b)		Material (c)		Material (d)	
	$\beta_y$	$\beta_p$	$\beta_E$	$\beta_{y,eff}$	$\beta_{E,eff}$	$\beta_y$	$\beta_E$	$\beta_{ye}$	$\beta_E$
20	1.00	1.00	1.00	1.00	1.00	1.00	1.00	1.00	1.00
100	1.00	1.00	1.00	1.00	1.00	1.00	1.00	1.00	1.00
200	1.00	0.81	0.90	0.89	0.84	1.00	0.90	0.88	0.90
300	1.00	0.61	0.80	0.79	0.68	1.00	0.80	0.77	0.80
400	1.00	0.42	0.70	0.69	0.54	1.00	0.70	0.67	0.70
500	0.78	0.36	0.60	0.56	0.47	0.78	0.60	0.54	0.60
600	0.47	0.18	0.31	0.32	0.24	0.47	0.31	0.31	0.31
700	0.23	0.08	0.13	0.15	0.10	0.23	0.13	0.14	0.13
800	0.11	0.05	0.09	<sup>a</sup>	<sup>a</sup>	0.11	0.09	0.07	0.09

<sup>a</sup>These are not provided by Agarwal and Varma (2011).

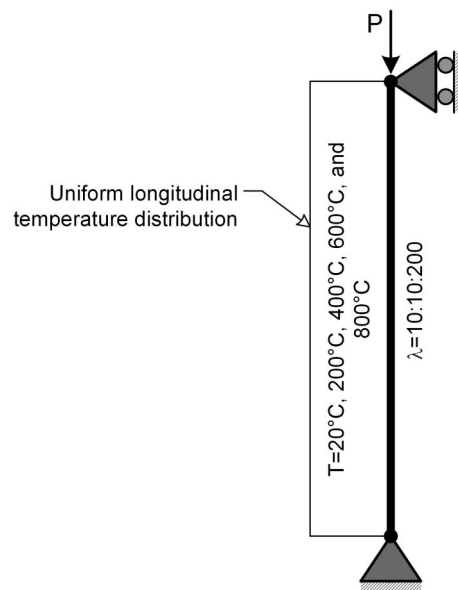


**Fig. 6.** Details of column member analyzed under uniform ambient and elevated temperatures

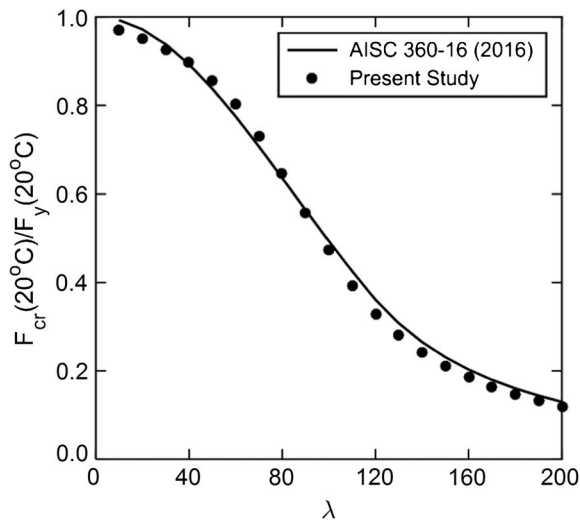


**Fig. 7.** Buckling stress computed using *AISC 2016 Specification* [AISC 360-16 (AISC 2016)] and proposed formulation in present study

### Uniform Longitudinal Ambient Temperature: Pinned–Pinned Column

At ambient temperature, the results of the analysis are compared to the column buckling stress,  $F_{cr}$ , determined with Eqs. (25a)–(25c), in accordance with equations E3 and E4 of the *AISC 2016 Specification* [AISC 360-16 (AISC 2016)].

$$\text{For } \frac{KL}{r} \leq 4.71 \sqrt{\frac{E}{F_y}} \rightarrow F_{cr} = \left[ 0.658 \frac{F_y}{F_e} \right] F_y \quad (25a)$$

$$\text{For } \frac{KL}{r} > 4.71 \sqrt{\frac{E}{F_y}} \rightarrow F_{cr} = 0.877 F_e \quad (25b)$$

$$F_e = \frac{\pi^2 E}{\left( \frac{KL}{r} \right)^2} \quad (25c)$$

The *AISC 2016 Specification* [AISC 360-16 (AISC 2016)] equations for column buckling at ambient temperature are based on the assumption of elastic–perfectly plastic behavior of material. Therefore, the same material behavior is assumed in the verification at ambient temperature. Furthermore, while column initial out-of-straightness is considered, the effect of initial out-of-plumbness is neglected because it is not reflected in the *AISC 2016 Specification* [AISC 360-16 (AISC 2016)] column curve. As shown in Fig. 7, excellent agreement is observed between the critical buckling stress computed using the proposed formulation and that of the *AISC 2016 Specification* [AISC 360-16 (AISC 2016)] design equation.

### Uniform Longitudinal Elevated Temperatures: Pinned–Pinned Column

Two additional studies are chosen for further verification of column stability at elevated temperatures, utilizing the column buckling equations at elevated temperature, proposed by Takagi and Deierlein (2007) and Agarwal and Varma (2011). In fact, the equation for column buckling under uniform elevated temperature according to Appendix 4 of *AISC 2016 Specification*

[AISC 360-16 (AISC 2016)] is based on the equation proposed by the earlier study conducted by Takagi and Deierlein (2007) as shown by Eq. (26):

$$F_{cr}(T) = \left[ 0.42 \sqrt{\frac{F_y(T)}{F_e(T)}} \right] F_y(T) \quad (26)$$

where  $F_e(T)$  = Euler elastic buckling stress calculated by Eq. (25c) with the modulus of elasticity  $E(T)$  at (uniform) elevated temperature in the column. In both studies, a uniform temperature distribution along the length of the pinned–pinned columns is assumed, initial out-of-straightness and residual stresses are considered, but the initial out-of-plumbness was not taken into account. Takagi and Deierlein (2007) utilized Material Model (a) in accordance with Fig. 5(a) while Agarwal and Varma (2011) implemented Material Model (b). Making the same assumptions as in the two previous studies allows for a direct comparison with the results of those studies.

The comparison is conducted at four various temperatures: 200, 400, 600, and 800°C. In this comparison, the proposed design equations by Takagi and Deierlein (2007) and Agarwal and Varma (2011) are plotted first for each of the above-mentioned temperatures. Then, using each of the four temperature-dependent Material Models (a)–(d) discussed in the previous section, a nonlinear finite-element analysis was conducted. Fig. 8 shows good agreement between the results obtained using the proposed finite-element formulation and the results achieved using the equations proposed in the two above-mentioned studies at all temperatures. Thus, the results of the proposed methodology against previous studies, which utilized commercial finite-element software with shell elements, clearly demonstrates the efficiency of the proposed approach and highlights its potential as an attractive alternative to evaluate stability of columns at elevated temperatures.

This study has confirmed the results of previous analyses (Takagi and Deierlein 2007; Agarwal and Varma 2011), which showed that the use of elastic–perfectly plastic temperature-dependent material behavior results in nonconservative estimates of buckling stresses. Moreover, Fig. 8 shows that the proposed tri-linear temperature-dependent material behavior in the present study provides very good agreement with the previous studies, particularly with the results of Agarwal and Varma (2011). The calculated buckling stresses using the proposed stability analysis framework are in good agreement, overall, with those found in previous studies. Since Material Models (b)—proposed by Agarwal and Varma (2011)—and (d)—proposed in this study—provide similar results, further analysis on evaluating the effect of initial lateral demand is conducted using Material (d).

### Case Study 1: Effect of Boundary Conditions Using Uniform Longitudinal Temperatures

As previously discussed, the effects of boundary condition on buckling of steel columns at elevated temperatures can be captured using the proposed formulation. To illustrate this capability, two various boundary conditions are considered including fixed–fixed and fixed–pinned as shown in Fig. 9. The fixed–fixed column is analyzed under uniform ambient temperature and 400°C as shown in Fig. 9(a). The fixed–pinned column is evaluated under uniform temperatures of 200 and 600°C as shown in Fig. 9(b).

The results of the fixed–fixed column subjected to uniform ambient temperature are compared to current *AISC 2016 Specification* [AISC 360-16 (AISC 2016)], Eq. (25), as shown in Fig. 10. It is noted that the effective length factor of 0.5 is employed in the available equations because of the fixed–fixed boundary condition.



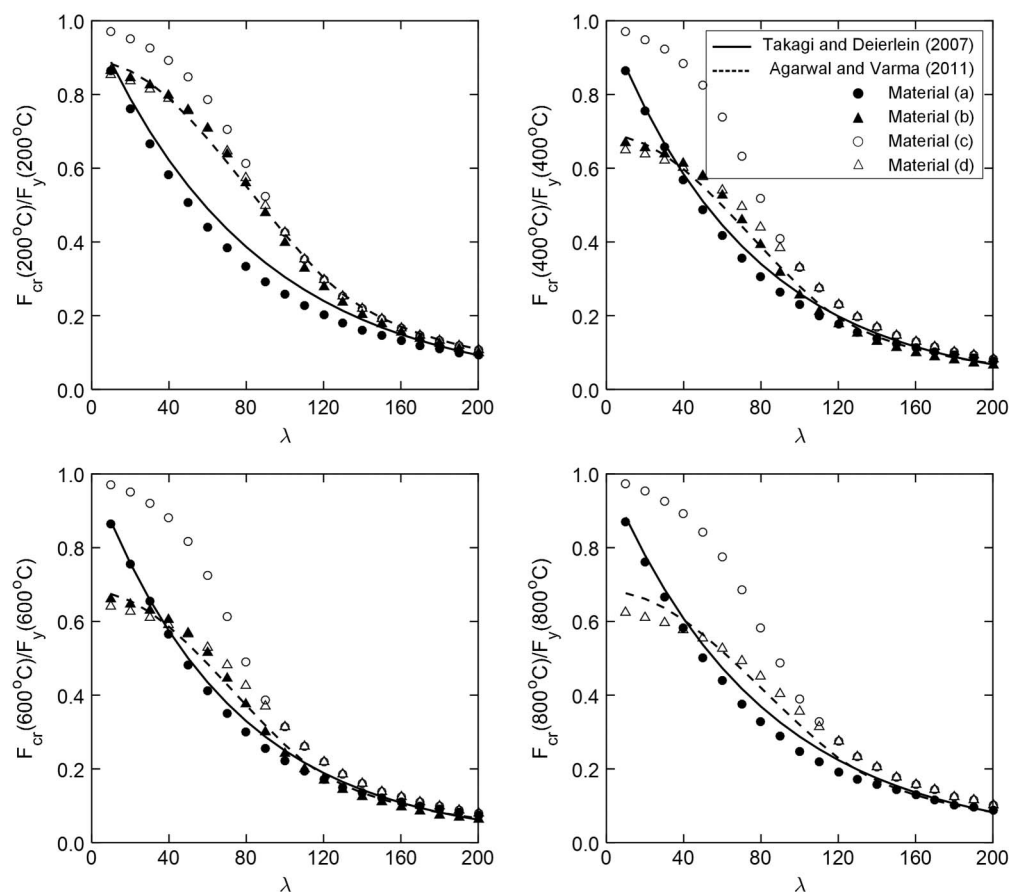


**Fig. 8.** Buckling stress of steel columns subjected to uniform longitudinal temperature using nonlinear finite-element analysis presented in this study versus proposed design equations

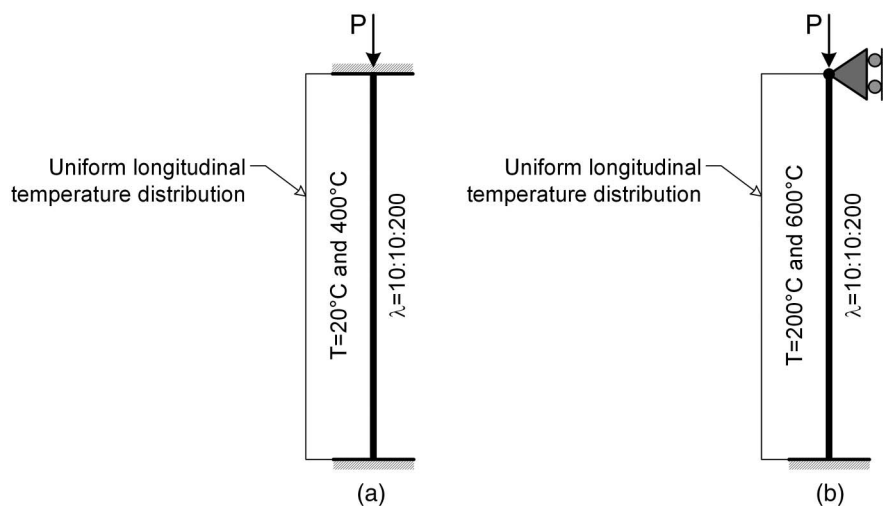


**Fig. 9.** (a) Fixed–fixed column with uniform longitudinal ambient and 400°C temperatures; (b) fixed–pinned column with uniform longitudinal 200 and 600°C

An excellent agreement is observed between the proposed formulation and the *AISC 2016 Specification* [AISC 360-16 (AISC 2016)]. The fixed–fixed column with the uniform longitudinal temperature of 400°C is analyzed using Materials (a)–(d) and the results are compared to the results of Takagi and Deierlein (2007) and Agarwal and Varma (2011). As shown in Fig. 10, good agreement is observed between the results for the formulation using

Material (a) and Takagi and Deierlein (2007). In addition, the results of Materials (b) and (d) show a good agreement with Agarwal and Varma (2011) as shown in the same plot. The results obtained using Material (c) show nonconservative prediction of buckling stress as observed in the validation study as well.

The fixed–pinned column with the uniform longitudinal temperatures of 200 and 600°C is also analyzed using Materials (a)–(d).

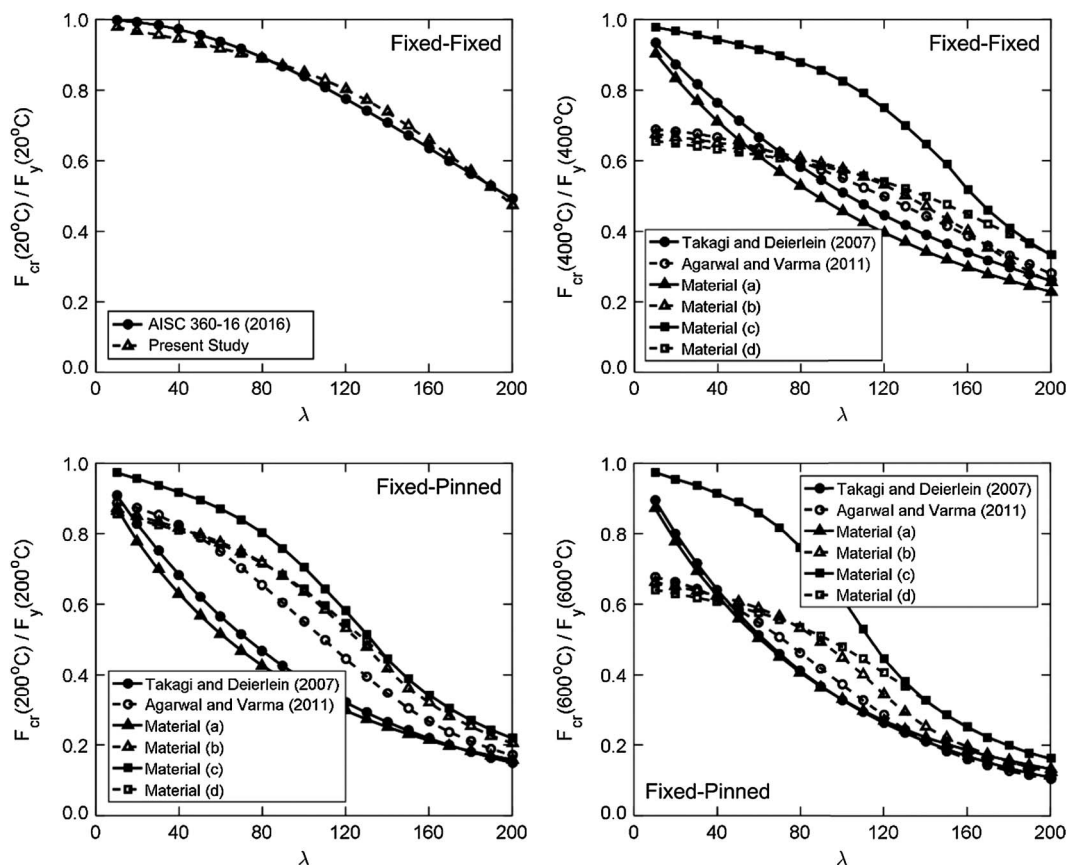


**Fig. 10.** Critical buckling stress of steel columns subjected to uniform longitudinal temperatures considering various boundary conditions

In this case, an effective length factor of 0.8 is implemented in the available equations. As shown in Fig. 10, it is observed that the buckling stress calculated using Material (a) is in excellent agreement with those calculated using Takagi and Deierlein (2007). Moreover, the results for analysis for Materials (b) and (d) are in a close agreement with the results using the equation proposed by Agarwal and Varma (2011). Material (c) also does not show a good performance in this case study similar to validation analysis.

### Case Study 2: Effect of Interstory Drift Followed by Uniform Longitudinal Temperature

To emulate the multi-hazard effect of lateral demand on a column resulting from an earthquake followed by fire loading, an analysis is conducted to evaluate the instability of pinned–pinned columns exposed to uniform temperatures along the column length, with and without interstory drift. The interstory drift represents a level of residual drift that might be experienced by a column at the conclusion of an earthquake event. For a typical steel moment frame, e.g., located in San Francisco, the drift limits used in this case study might correspond to a state of substantial but repairable damage with a return period of about 400–500 years. To establish context, a residual drift of 1% might arise from an earthquake with a return period of 500 years. It is emphasized that the analysis conducted in the present study is aimed at highlighting the capabilities of the proposed framework in addressing stability effects under combined hazards. Further studies are needed to fully assess such loading demand. For example, evaluating the response of an isolated column, with idealized pinned–pinned boundary conditions, does not

provide the same level of insight that could be achieved from a frame analysis. Furthermore, while it is recognized that structural deterioration due to reversals of inelastic deformation during an earthquake may occur, the hysteresis loops of properly designed steel moment frames are relatively stable, and the deterioration in strength and stiffness would be less than the deterioration at elevated temperatures indicated by Table 1.

As shown in Fig. 11(a), four uniform temperatures are considered in the analysis—200, 400, 600, and 800°C along the column length. Materials (a) and (d), in accordance with Fig. 5, are utilized in the analysis to investigate their effects on the response of columns subjected to various levels of interstory drift and temperatures. First, the columns are analyzed with no interstory drift as shown in Fig. 11(b). Second, two levels of lateral sway are applied to the columns:  $\Delta = 0.01L_c$  and  $\Delta = 0.02L_c$  as shown in Fig. 11(c).

Fig. 12 shows the results of the analyses of the above columns. The inclusion of interstory drift causes a significant reduction in the stress at instability of pinned–pinned steel columns, as might be expected. Furthermore, Material (d) generally resulted in larger instability stresses for columns with no interstory drift in comparison to Material (a) except at slenderness values,  $\lambda$ , smaller than 40. However, when interstory drift is included, Material (d) always resulted in relatively smaller instability stresses than those obtained using Material (a).

The minimum reduction in the instability stress in the presence of interstory drift appears to occur in the shortest steel columns, with  $\lambda = 10$ . The reduction is 50–55% for 1% interstory drift and 65–70% for 2% interstory drift for both Material Models (a) and (d). The maximum reduction in instability stress due to interstory

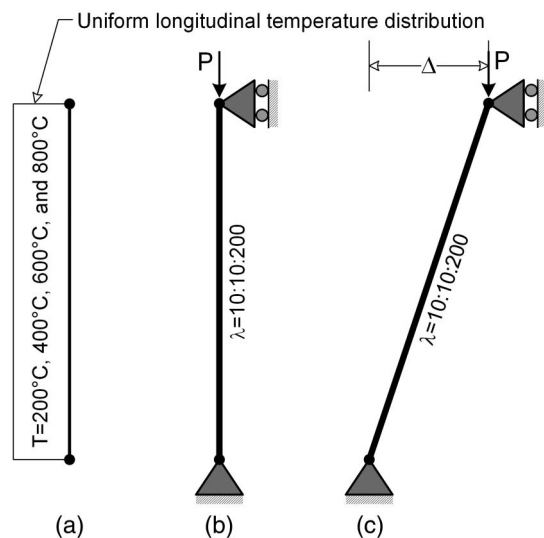


**Fig. 11.** (a) Uniform temperature distribution in columns; (b) pinned-pinned columns with various slenderness ratios and no residual interstory drift; (c) pinned-pinned columns with various slenderness ratios and subjected to lateral sway at two levels of  $\Delta = 0.01L_c$  and  $\Delta = 0.02L_c$

drift occurs in columns in the slenderness range between 50 and 100 ( $50 \leq \lambda \leq 100$ ). For 1% interstory drift, Material (a) results in 70–80% reduction in the instability stress while an 80–90% reduction is seen using Material (d). Not surprisingly, these reductions

increase at an interstory drift of 2%. The reduction in the instability stress caused by the interstory drift is minimal for slenderness ratios larger than 100 ( $\lambda > 100$ ), where the column behavior is approaching the elastic condition.

### Case Study 3: Effect of Interstory Drift and Nonuniform Longitudinal Temperature

The proposed stability formulation has the capability to analyze columns under temperature profiles that are nonuniform along the column length; this is one of its distinctive features when compared with previous column analyses. Two nonuniform longitudinal linear temperature profiles, shown in Figs. 13(a and b), are chosen to illustrate this capability. Temperature Profile 1 has minimum and maximum temperatures of 300 and 600°C, respectively, shown in Fig. 13(a), while Temperature Profile 2 starts from 400°C at one end and rises up to 800°C at the other end, shown in Fig. 13(b). Columns in this illustration of nonuniform longitudinal temperature effects are analyzed without interstory drift, Fig. 13(c), and with 1% drift,  $\Delta = 0.01L_c$ , as shown in Fig. 13(d). The effects of material stress-strain modeling are also considered.

As shown in Fig. 14, columns with interstory drift have significantly smaller stresses at instability than those with no lateral drift. When the columns are not subjected to interstory drift and column slenderness ratios exceed approximately 100 for both temperature profiles, the instability stress is larger when Material (d) is used. Conversely, Material (a) results in a larger instability stress than that of Material (d) when the interstory drift of the columns equals 1%. Both Material Models (a) and (d) lead to approximately

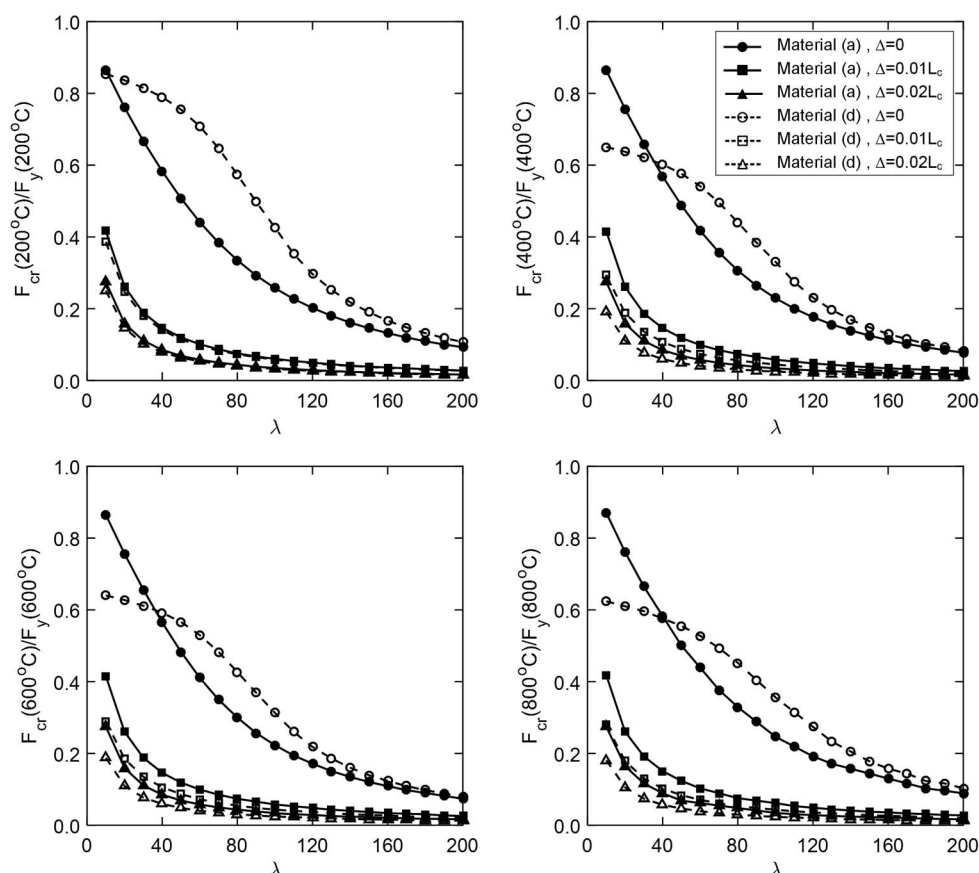


**Fig. 12.** Instability stress of steel columns subjected to uniform longitudinal temperature with and without lateral drift

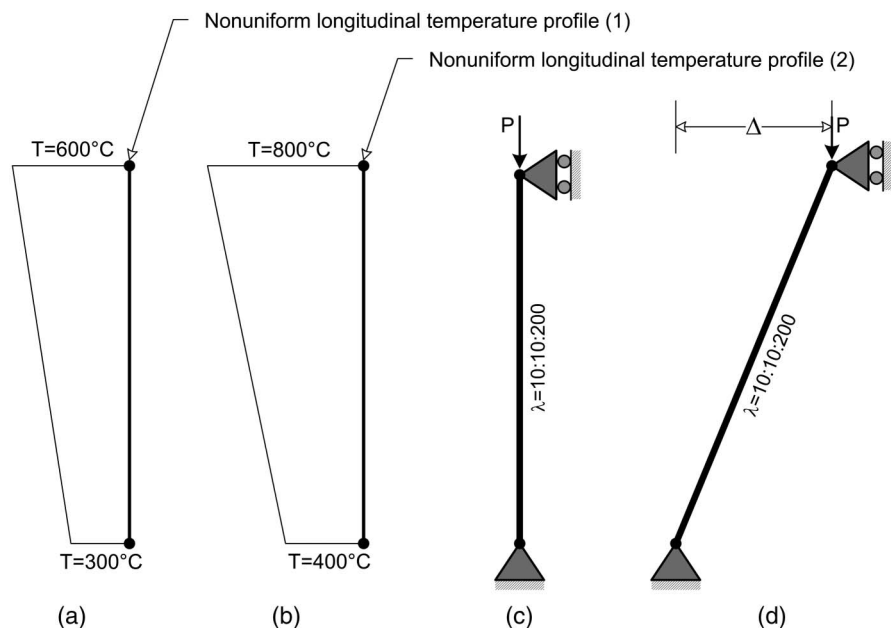


**Fig. 13.** (a) Nonuniform longitudinal Temperature Profile 1; (b) nonuniform longitudinal Temperature Profile 2; (c) pinned-pinned columns with various slenderness ratios and no residual interstory drift; (d) pinned-pinned columns subjected to lateral sway of  $\Delta = 0.01L_c$

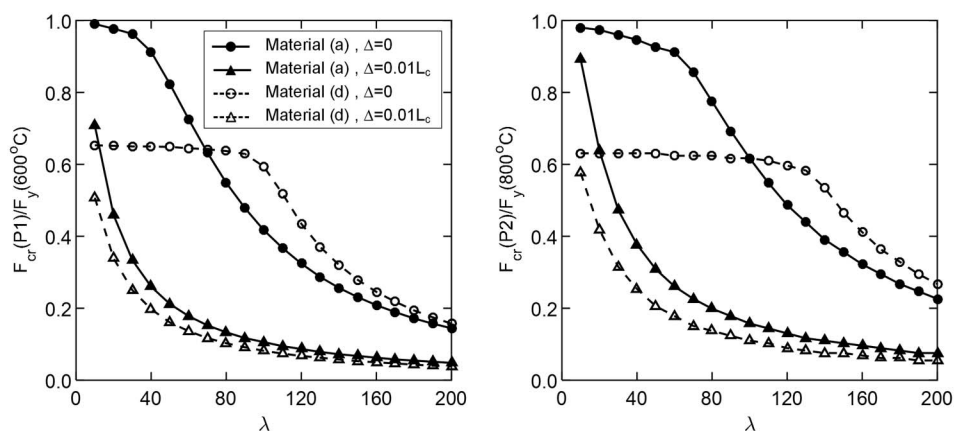


**Fig. 14.** Instability stress of steel columns subjected to nonuniform longitudinal temperature with and without interstory drift

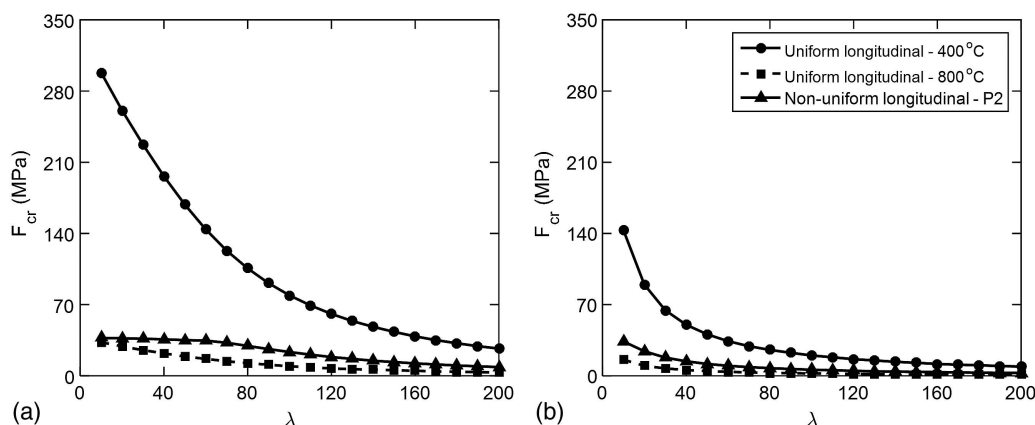


**Fig. 15.** Comparison between uniform and nonuniform longitudinal temperature profiles: (a) without and (b) with lateral sway of  $\Delta = 0.01L_c$



identical reductions in the instability stress for slenderness ratios equal to or less than 60 ( $\lambda \leq 60$ ) for each of the temperature profiles.

#### Case Study 4: Effect of Uniform versus Nonuniform Longitudinal Temperature

This section evaluates the difference between uniform and non-uniform longitudinal temperature profiles using the proposed formulation. In this case, two uniform longitudinal temperature distributions, 400 and 800°C, are selected. Profile 2 per Fig. 13(b) is considered for nonuniform temperature distribution since its temperature profile varies between 400 and 800°C. Columns with pinned–pinned boundary conditions with Material (a) are only considered. The analysis is performed for columns with no interstory drift and with 1% drift,  $\Delta = 0.01L_c$ .

Fig. 15(a) shows the results of the case with no interstory drift. It is seen that the stress at the onset of instability for the column with uniform longitudinal temperature distribution of 800°C is smaller compared to that with nonuniform longitudinal temperature Profile 2, varying from 400 to 800°C. The same pattern is observed when the column is initially subjected to 1% drift, shown in Fig. 15(b). This is attributed to the fact that column with nonuniform longitudinal temperature distribution, Profile 2, has variable, however overall larger, mechanical properties along the length compared to the column with uniform temperature profile of 800°C. The results highlight the need for conducting analysis using the proper temperature distribution since a direct relationship between the results obtained using uniform and nonuniform distributions cannot be inferred.

#### Summary and Conclusions

In this study, a nonlinear stability formulation was developed to assess the response of steel columns under the sequential demand of earthquake and fire loads. The proposed approach is seen as a tool that can be utilized to study the effects of a wide variety of variables on the instability of steel columns subjected to fire following earthquakes or fire loads acting alone. This methodology includes both  $P$ - $\delta$  and  $P$ - $\Delta$  effects, residual stresses in hot-rolled  $W$ -shaped steel sections, temperature-dependent material modeling, different boundary conditions, and nonuniform temperatures along the length of the steel columns. Good agreement was observed between results of the proposed formulation and available strength design equations for steel columns at ambient and elevated temperatures. The following preliminary conclusions can be drawn from the analyses:

- The method showed excellent agreement with Chapter E of the *AISC 2016 Specification* [AISC 360-16 (AISC 2016)] for ambient temperatures.
- Using temperature-dependent material modeling in *Eurocode 3* (CEN 2005), good agreement with the results of Takagi and Deierlein (2007) was obtained.
- The proposed approach resulted in close agreement with the design equation proposed by Agarwal and Varma (2011) when implementing their material model.

- The assumption of elastic–perfectly plastic steel behavior at elevated temperatures results in nonconservative instability stresses.
- The inclusion of interstory drift with uniform longitudinal temperature results in significant reduction in buckling capacity of steel columns. This effect is not considered in the Appendix 4 provisions of the *AISC 2016 Specification* [AISC 360-16 (AISC 2016)].
- The use of nonuniform longitudinal temperature resulted in the maximum reduction in instability stress caused by lateral drift effects in columns with slenderness ratios exceeding approximately 100.
- Comparison between uniform and nonuniform longitudinal temperature distributions highlight the need for using the proper temperature distribution since a direct relationship between the results cannot be inferred.

#### References

- Agarwal, A., Choe, L., and Varma, A. H. (2014). “Fire design of steel columns: Effects of thermal gradients.” *J. Constr. Steel Res.*, 93, 107–118.
- Agarwal, A., and Varma, A. H. (2011). “Design of steel columns at elevated temperatures due to fire: Effects of rotational restraints.” *Eng. J.*, 48(4), 297–314.
- AISC. (2005). “Steel construction manual.” *AISC 360-05*, Chicago.
- AISC. (2010). “Steel construction manual.” *AISC 360-10*, Chicago.
- AISC. (2016). “Steel construction manual.” *AISC 360-16*, Chicago.
- Ali, F., and O'Connor, D. (2001). “Structural performance of rotationally restrained steel columns in fire.” *Fire Saf. J.*, 36(7), 679–691.
- ASTM. (2015). “Standard specification for structural steel shapes.” *A992/A992M*, West Conshohocken, PA.
- Carol, I., and Murcia, J. (1989). “Nonlinear time-dependent analysis of planar frames using an exact formulation. I: Theory.” *Comput. Struct.*, 33(1), 79–87.
- CEN (European Committee for Standardization). (2005). “Design of steel structures. Part 1.2: Structural fire design.” *Eurocode 3*, Brussels, Belgium.
- Franssen, J. M., Talamona, D., Kruppa, J., and Cajot, L. G. (1998). “Stability of steel columns in case of fire: Experimental evaluation.” *J. Struct. Eng.*, 10.1061/(ASCE)0733-9445(1998)124:2(158), 158–163.
- Memari, M., and Attamejad, R. (2010). “An innovative Timoshenko beam element.” *Proc., 10th Int. Conf. on Computational Structures Technology*, Civil-Comp Press, Stirlingshire, U.K.
- Memari, M., and Mahmoud, H. (2014). “Performance of steel moment resisting frames with RBS connections under fire loading.” *Eng. Struct.*, 75, 126–138.
- Memari, M., Mahmoud, H., and Ellingwood, B. (2014). “Post-earthquake fire performance of moment resisting frames with reduced beam section connections.” *J. Constr. Steel Res.*, 103, 215–229.
- Phan, L. T., McAllister, T. P., Gross, J. L., and Hurley, M. J. (2010). “Best practice guidelines for structural fire resistance design of concrete and steel buildings.” *NIST Technical Note 1681*, National Institute of Standards and Technology, Gaithersburg, MD.
- Takagi, J., and Deierlein, G. G. (2007). “Strength design criteria for steel members at elevated temperatures.” *J. Constr. Steel Res.*, 63(8), 1036–1050.
- Tan, K. H., and Yuan, W. F. (2009). “Inelastic buckling of pin-ended steel columns under longitudinal non-uniform temperature distribution.” *J. Constr. Steel Res.*, 65(1), 132–141.
- Vandamme, M., and Janss, J. (1981). “Buckling of axially loaded steel columns in fire conditions.” *IABSE Proc., P-43/81, IABSE Periodica 3/1981*, E-Periodica, ETH Zurich, Switzerland, 81–95.